USE OF A NEW IMPEDANCE CELL AND 3D MRI TO OBTAIN FAST AND ACCURATE RESISTIVITY INDEX MEASUREMENTS FROM A SINGLE CENTRIFUGE STEP

N. Bona, B. Bam, M. Pirrone and E. Rossi
eni e&p

This paper was prepared for presentation at the International Symposium of the Society of Core Analysts held in Austin, Texas, USA 18-21 September, 2011

ABSTRACT

This paper presents a method for determining the Archie *n*-exponent from a single, non-equilibrium centrifuge step. The input measurements include detailed 3D saturation distributions from Magnetic Resonance imaging and the dc conductivity of the sample under examination. The latter is obtained by making use of a patented 4-contact cell that gives access to the entire sample volume and not only part of it. The sample is modelled as a 3D conductivity network and a fit-for-purpose algorithm based on Random Walk (RW) is used to compute its overall conductivity in a very short time. The *n*-exponent is determined by matching the measured conductivity to the calculated one. The entire analysis takes one day. Examples are presented to demonstrate the method. Details of the impedance cell as well as the RW algorithm are also given.

INTRODUCTION

Core-derived parameters for electric log calibration have a considerable impact on Hydrocarbon-In-Place estimations. Therefore, it is important to have many measurements of such parameters and make sure that they are as accurate as possible. The *n*-exponent is probably the most critical, because it is strongly affected by how evenly Sw is distributed in the sample. Achieving even Sw distributions takes a long time (months with the Porous plate and weeks with the Continuous injection), so results can arrive late for use in electrical log interpretation. The FRIM method [**1**] is much faster, but due to the particular electrode configuration that is used, only part of the sample volume is investigated. Non-invasive saturation monitoring makes it possible to detect non-uniform distributions of water saturation and (in theory) correct *n* accordingly. A method for doing the *n* correction was proposed by Jing et al. [**2**]. They use 1D saturation distribution data from gamma-ray or X-ray attenuation: the calculation is based on solving a model consisting of a series of slices that are assumed to have evenly-distributed saturations in them and the same type of electrical response. The individual resistances are additive, and *n* is derived by minimizing the difference between measured and calculated resistivity indices. Our method differs from this method in that we use 3D tomographic data and correct also for *m*. That makes the results more accurate, for in general porosity is not constant throughout the sample and Sw does not vary only along the length of the sample but also in transverse directions.

OUTLINE OF THE METHOD

Our method relies upon the acquisition of two 3D MR images of the sample under examination. The images are taken under fully water saturated conditions and after a short centrifuge step (in air or oil). The low resolution of the images (typically 2 mm cubic) makes their acquisition rather fast. The images are processed and two cubic networks are generated: these represent the two saturation states of the sample and have a MR-derived porosity Φ_k and a MR-derived water saturation Sw_k assigned to each of the N voxels they consist of (k=1,2,...,N). Following Archie's equations (in principle other models can be used), the networks are then transformed into electrical conductivity networks. The conductivity assigned to the k-th voxel will depend on Φ_k and Sw_k and also on the values of the m and n exponents, which are assumed to be the same in all voxels. The overall networks' conductivities are then calculated by means of a Random Walk algorithm and the results compared to the experimental dc conductivities measured before and after centrifuging the sample. The m and n exponents are treated as matching parameters and represent the final output of our analysis.

EQUIPMENT AND PROCEDURES

Sample Desaturation. The desaturation of the sample is achieved by making use of a centrifuge. Because there is no need to establish a uniform saturation, the centrifuge is suitable for this scope. A Free Water Level can be put at the base of the sample. In so doing, a wider Sw spectrum is generated (values will range from Sw_{min} to 1) and the resulting n will capture a larger portion of the RI vs. Sw relationship. The amount of capillary pressure we put on the sample during desaturation is not very high. The average Sw in the sample is measured by weighing.

Electrical Measurement and the Impedance Cell. Sample electrical conductivity is measured before and after centrifuging. These measurements are very fast (minutes), stable and repeatable. They are performed at ambient conditions using a patented 4-contact cell [**3**] that allows us to measure the conductivity of the entire sample. Being able to measure the whole sample is a necessary requirement with our method. It also represents a clear advantage in common practice, as pointed out by Lasswell [**4**]. **Fig.1** shows three pictures of the cell. All the contacts are placed on the faces of the sample. The V^+/I^+ and V^-/I^- electrode pairs are identical. In each pair, the electrode for the measurement of the voltage is concentric to the current electrode. The cell has been designed in such a way that the electric field and the current density inside the sample are uniformly distributed and independent of the size and the electrical characteristics of the sample. An example of the potential generated in the sample during testing is illustrated in **Fig.2**. When measuring, the cell is connected to the Novocontrol Alpha impedance analyzer, equipped with the ZG4 interface [**5**]. The measurement circuit is schematized in **Fig.3**. Like 2-contact measurements, also 4-contact yield resistance values that may differ from the true resistances. The two types of measurements are, in a certain sense, complementary: 2-contact techniques suffer from large errors when low-resistance samples are measured at low frequency; 4-contact methods may have problems with high-resistance samples tested at high frequency. However, in general 4-contact methods

are superior. **Fig.4** shows that in 4-contact measurements, errors (if present) are negative, i.e. the rock resistance is underestimated. The most critical factors are the resistance of the rock and the resistance of the voltage electrode/rock contact. Large errors can affect a 4-contact measurement if one (or both) of these resistances is large. There is an obvious effect on the *n* exponent. During a Resistivity Index (RI) measurement in which Sw is progressively reduced, the resistance of the rock becomes increasingly large, and errors may start being significant. Since they depend on the resistance of the rock, not only an erroneous *n* value might be obtained but also the measured RI curve might no longer appear as a straight line. **Fig.4** compares our experimental setup to the classic 4-contact setup in which the voltage difference is measured using two lateral rings pressed against the sample [**6**]. As can be seen, measurement errors are smaller with our system. It should be noted that errors do not depend only on the geometry and position of the electrodes, but also on how current and voltage are measured (i.e. on the measurement circuit).

Sample Imaging and Φ-Sw Derivation. Our MRI system is the Bruker Biospec 24/40 image spectrometer. It has a 2.4 T principal magnetic field and is equipped with gradients whose strength ranges from 50 to 200 mT/m. Maximum spatial resolution is 0.05 mm, but for the purpose of the present study a resolution (voxel size) of 2mm cubic was used. We find it the best compromise between two opposite needs: shortening analysis time and having homogeneous porosity and water saturation in each voxel. The sample is MR scanned after each electrical measurement. Due to the short scanning time (tens of minutes), there are not relevant fluid redistributions inside the sample. A critical point is the positioning of the sample inside the imager. Because we compare the image acquired at Sw=100% to the desaturated image on a voxel-by-voxel basis, it is essential that the sample is exactly in the same position. The largest tolerable error is a few tenths of mm. The calculation of the porosity and water saturation distributions is a three-step process:

1. *MR data acquisition and pre-processing*. The MR data are obtained from a 15 echo-CPMG sequence. The echo-time is the shortest possible with our system, i.e. 2.46 ms. As a result, at the moment only samples with T_2 times longer than a few ms can be safely tested, which excludes, for instance, rocks with high iron/manganese concentrations; MR sequences able to give echo-times on the order of 50 μs or less are currently under examination. Once the MR acquisition has been completed, we calculate the zero-time limit of the T_2-decay curves measured in each of the voxels (the fitting functions are single exponentials). Since the resulting numbers represent a measure of the initial magnetizations of the voxels, they are used as preliminary estimates of voxels' water contents. Let A_k be the value assigned to the k-th voxel at Sw=100%, and B_k the value obtained under partial Sw.
2. *Quality check.* Each voxel is assigned a porosity and a preliminary Sw. The k-th voxel porosity is defined as: $\Phi_k = \Phi N A_k / \sum A_k$ (where N is the total number of voxels and Φ is the total porosity of the sample). The k-th voxel water saturation is given by: $Sw_k = B_k/A_k$. The average MR-derived water saturation of the sample (i.e. the quantity $\sum(B_k/A_k)/N$) is then compared to the experimental value obtained by weighing the sample before and after centrifuging. Typically, we observe differences that are on the order of a few saturation units: the MR-derived Sw is almost invariably

underestimated and the lower the water saturation of the sample the larger the discrepancy. These systematic errors are probably due to the fact that in spite of the short echo-time that is used, the shortest T_2 components are not entirely captured and part of the water in the sample is consequently missed. If there is more than a 20%-difference between the MR-derived average Sw and the Sw from sample weight, the analysis is stopped and the sample rejected. We also stop the analysis if the MR-derived average Sw is higher than the Sw from weight.

3. *Sw correction.* Those samples that meet the aforementioned requirements gain access to this third phase. MR-derived water saturations always need a correction. The Sw correction consists of two steps. First, since a limited number of voxels might have A_k and B_k values such that $A_k<B_k$ (which is not acceptable), all the B_k numbers are replaced by $C_k = min(A_k; B_k)$. Then, every C_k is multiplied by a factor f_k defined as $f_k = [1+ \alpha(A_k/C_k–1)]$. The α constant is determined by forcing the MR-derived average saturation of the sample to equal the saturation from weight, i.e. by minimizing the objective function $\left| Sw_{weight} - \sum f_k(C_k/A_k)/N) \right|$. The calculation of α is quite simple because there are no local minima in the objective function, and the resulting Sw_k network generally looks fine. Notice that f_k tends to 1 as $C_k \rightarrow A_k$ and increases as the C_k/A_k ratio decreases. That reflects the observation that relative errors in the estimated saturations increase when *Sw* decreases. We do not perform any correction on A_k. The *k*-th voxel is eventually assigned the corrected saturation $Sw_k = f_kC_k/A_k$, and the porosity $\Phi_k = \Phi NA_k/\sum A_k$.

Conductivity Networks and m/n Calculation. Once Φ_k and Sw_k have been defined, each voxel is assigned the fully saturated electrical conductivity $\sigma_{0k} = \sigma_w\Phi_k^m$ and the partially saturated conductivity $\sigma_{tk} = \sigma_w\Phi_k^m Sw_k^n$, where σ_w is the conductivity of the saturant water. In this paper, rock conductivity is supposed to be properly described by Archie's laws. It is also assumed that porosity and water saturation are evenly distributed within each voxel, and that all voxels have the same *m* and *n* values. The first step is to select a number (typically 10) of *m*-values centred around the expected *m*-exponent. Then, a Random Walk algorithm is used to compute the overall conductivity of the fully saturated network in a short time for each of the selected *m*'s. Network conductivity is a monotonically decreasing function of *m* and a suitable power law can be easily extracted by standard fitting techniques (**Fig.5a**). Once the $\sigma_{0k}(m)$ curve has been defined, we enter it with the experimental conductivity measured before centrifuging and get the corresponding *m* value. This is the first output of the process. The *m*-exponent thus obtained is then substituted into the σ_{tk} relation. The second step is analogous to the first one: ten values of *n* around the expected value are selected. The Random Walk algorithm is run again to compute the $\sigma_{tk}(n)$ relationship and this is fitted with another power law. The resulting curve is entered with the conductivity measured on the sample after centrifuging and the corresponding *n* extracted.

Random Walk Algorithm. The algorithm we use is an extension of the "ant in a labyrinth" random walk algorithm, which simulates the diffusion of non-sorbing species in pore networks. This approach provides a useful description of electrical transport in

disordered systems exploiting the Einstein's relation between conductivity σ and diffusion coefficient D, namely $\sigma = nq^2D/(kT)$, where n is the effective number density of charge carriers, q the elementary charge, k the Boltzmann constant and T the temperature. Following Einstein's relation, in a rock the diffusion coefficient is assumed to be intimately connected to conductivity via the relation $\sigma/\sigma_w = \phi S_w D/D_w$, where σ and σ_w are the rock and saturant water conductivities, D_w is the diffusion coefficient of bulk water (often fixed to unity), Φ is the porosity and S_w the water saturation.
The diffusion coefficient is calculated numerically by using a set of random walkers travelling in the 3D conductivity lattice and by computing their mean-square displacements in the long-time limit. More precisely, D is given by the equation $\langle r^2(\tau)\rangle \approx D\tau$ at large dimensionless integer time τ, where $\langle r^2(\tau)\rangle$ is the mean-square distance travelled by the random walkers at time τ. Natural rocks often possess anisotropic pore structures and characteristics, so that D is a tensor and directional mean-square displacements $\langle x^2\rangle$, $\langle y^2\rangle$ and $\langle z^2\rangle$ are needed (**Fig.5b**). In order to properly consider the heterogeneity of the probed rock, the single walker migrates on discrete voxels whose grey-levels correspond to the conductivity network. All conductivities are normalized so that $\sigma_k = \sigma_k/\sigma_{max}$. The random walker at site k chooses one of its six nearest neighbours, say j, at random (i.e. with a probability equal to 1/6), and moves there with a probability given by $p_{kj} = 2\sigma_k\sigma_j/(\sigma_k+\sigma_j)$ or stays with probability $(1-p_{kj})$. In either case, the simulation time is incremented by one unit. The form of p_{kj} is suggested by the fact that for flow in one dimension, or for flow perpendicular to the layers in a layered medium, the effective conductivity is given by the harmonic mean of the constituent conductivities [**7**]. Mirror boundary conditions [**8**] are used.

RESULTS AND DISCUSSION

We discuss the experiments conducted on two rock samples: a Berea sandstone having a permeability of 720 md and a porosity of 21.5%, and a laminated sandstone with a permeability of 8.8 md and a porosity of 17.0%. Both samples are rectangular parallelepipeds with a square base (this unusual shape makes it easier to control the position of the sample inside the MR imager with a high degree of precision, but also cylindrical samples can be analysed). Heights and base sides are approx. 4.5 and 2 cm, respectively. All determinations were made at ambient conditions. The samples were measured for Archie-n using the conventional procedure and then n was re-determined using the new approach.

Berea sandstone. **Tab.1** and **Fig.6-7** summarize the results obtained on the Berea sample. **Fig.6** illustrates the resistivity index curve measured using an air-water primary drainage porous plate experiment. The resulting n-exponent is 1.55 and we will consider this value as the reference. On completion of the classic RI measurement, the sample was cleaned, dried and re-saturated with the same brine (salinity: 52 g/l NaCl; conductivity at 20°C: 6.40 S/m). Then, the fully-saturated electrical conductivity of the sample was measured and a MR image acquired. The image was transformed into a 3D porosity map and this porosity map into a conductivity network. The RW algorithm was run and the resulting

average network conductivity matched to the measured sample conductivity. A *m*-exponent of 1.58 was eventually obtained. The value calculated from the standard formula $m = -\log(\sigma_w/\sigma_0)/\log(\Phi)$ was 1.62. Then, the following steps were made:

a) The sample was centrifuged with a Free Water Level put at its base. The rotational speed was set so that the capillary pressure at sample mid-point was 0.3 bars. After a few hours, the centrifuge was stopped, the sample weighed, its partially-saturated electrical conductivity measured, and a second MR image acquired. From this, a 3D saturation map was generated (**Fig.7a** shows a projection on a vertical plane). Notice that a clear Sw gradient existed along the sample length. After running the RW algorithm, a *n*-exponent equal to 1.51 was obtained. The standard formula $n = -\log(\sigma_0/\sigma_t)/\log(Sw)$, which assumes an even saturation distribution inside the sample, gave n=1.75.
b) Then, the sample was laid down into a beaker containing a certain amount of brine (approx. 1/3 of the sample laid below the water level, the rest of the sample was in air). Water imbibition lasted 1.5 hours, after which another conductivity measurement and a new MR acquisition were made. The resulting saturation map (actually, its 2D projection) is shown in **Fig.7b**. As can be seen, the upper part of the sample now exhibits quite an even saturation distribution, but the high Sw region generated at the bottom while centrifuging is still present. A *n*-exponent of 1.50 was obtained from the RW calculation, at this step. The standard formula gave n=1.46.
c) Finally, the sample was re-centrifuged under the same conditions as before, but without a FWL. Then, it was laid down again into a beaker, this time for 20 seconds only, and with a lower amount of water (the water covered only 1/10 of the sample). After this short imbibition, sample weight, electrical conductivity and another MR image were acquired. The corresponding saturation map is shown in **Fig.7c**. The Sw gradient along the sample length disappeared, and a small transverse gradient (caused by the incomplete water imbibition) formed in the upper part of the sample. The *n*-exponent obtained after running the RW algorithm was 1.60. The standard formula gave n=1.61 (since Sw was distributed in a relatively even way, a good agreement between the two *n* values was obtained).

	Porous Plate	a	b	c
n	1.55	1.51	1.50	1.60

Tab.1 – n-values obtained on a Berea sample from the conventional porous plate test and the proposed method. a) after centrifuging; b) after a long water imbibition; c) after a short imbibition.

The *n* exponents calculated using the new approach were found to be rather independent of the degree of homogeneity of the Sw distribution inside the sample, considering the various sources of uncertainty in the proposed workflow. Moreover, all the calculated *n*'s were close to the value obtained from the classic porous plate test. That demonstrates that reliable measurements of *n* can be obtained even under non-equilibrium saturation conditions. The standard method, on the contrary, gave more scattered results, consistently with the fact that it can be applied only in the presence of even Sw distributions.

Laminated sandstone. The second example refers to a "difficult" sample with a low MR signal/noise ratio. **Fig.8** illustrates the Resistivity Index curve obtained from an air-brine porous plate desaturation. Even though the clay content of the sample is low and an Archie behavior should consequently be expected, we measured a *n*-exponent equal to 1.15, a value that is well below the standard 2.00. This result is due to the laminated structure of the rock, which consists of fine-grained/coarser sand alternances (we will come back to this point later). After the conventional RI measurement, the sample was cleaned, dried and re-saturated (brine salinity: 172 g/l NaCl; brine conductivity at 20°C: 18.3 S/m). Then, it was centrifuged under air (no FWL; mid-point capillary pressure = 2 bars). **Fig.9a** shows a 2D projection of the 3D porosity map obtained from the MRI data. The *m*-exponent after running the RW algorithm was found to be 1.81; the standard formula ignoring porosity heterogeneity gave *m*=1.85. The saturation map acquired after centrifuging (**Fig.9b**) shows diffused Sw unhomogeneities due to the lamination of the rock and a weak longitudinal Sw gradient caused by the centrifuge (capillary end-effect and Pc gradient). The *n*-exponent obtained after running the RW algorithm was 1.13. The standard formula gave *n*=1.21. Again, the proposed method provided a *n*-value that is consistent with the porous plate test result. It took more than one month to complete the porous plate experiment, while one day was enough to obtain *n* with the new method. **Tab.2** summarizes the results.

	Porous Plate	New method
n	1.15	1.13

Tab.2 – n-values obtained from the conventional porous plate test and the method.

The very low *n* of this sample is imputable to the permeability contrast between the fine-grained and the coarse laminae. Because of their low permeability (and the correspondingly high threshold capillary pressure), the former remains fully water saturated during the desaturation of the sample. That assures a high overall electrical conductivity even if the average saturation of the sample becomes low, and explains the low *n* value that was measured. **Fig.10** illustrates better this point. Modeling the sample as a Sand#1/Sand#2 parallel combination and playing with the individual characteristics of the sands helps to understand this unusual experimental result. **Tab.3** shows one of the possible combinations of volume percentages, porosities, Sw's and Archie exponents allowing the reproduction of the experimental data.

	% of bulk Volume	Φ	Sw	m	n
Sand #1	50	14.0	90.0	1.70	1.80
Sand #2	50	19.9	17.5	2.00	2.04

Tab.3 – Sand1/sand2 parallel combination that matches the experimental data, namely: average porosity = 17.0%; average water saturation = 47.4%; average fully- and partially-saturated conductivities = 0.687 S/m and 0.278 S/m, respectively; brine conductivity = 18.3 S/m.

Interestingly, in both sands *n* is closer to 2. This has been confirmed also by measurements carried out on core plugs taken from less-thinly laminated intervals, where the sands could be sampled individually. The proposed method, therefore, may provide valuable help in handling upscaling issues. Incidentally, also *m* exhibits this type of

behavior: uneven porosity distributions yield *m* values that may differ significantly from those that would be measured if porosity was evenly distributed (**Fig.11**). Working on voxels of a few mm in size permits us to evaluate *m* and *n* at the so-called Representative Volume Element (RVE) scale. That is key to predicting the actual response of rock at larger scales.

CONCLUSIONS

A new method that combines electrical and 3D MRI determinations provides reliable measurements of the Archie-*n* exponent in the presence of non-equilibrium saturation distributions. Any type of Sw heterogeneity can be handled. The method works at ambient conditions and on consolidated rock. Compared to the classic porous plate and continuous injection methods, it is much faster (one day instead of weeks or even months). An essential element of the method is a 4-contact impedance cell in which current and voltage electrodes are placed all on the sample faces: this design minimizes the spurious impedances that normally affect an electrical measurement and enables the investigation of the whole sample volume. Also the *m* exponent is determined with the proposed method. Like the majority of petrophysical quantities, also *m* and *n* are scale-dependent. With the new method, they can be evaluated at the Representative Volume Element scale. That may be of great help in understanding the electrical behaviour of the probed rock at larger scales and represents a good starting point for possible upscaling work.

REFERENCES

1. Fleury, M.: “FRIM, a fast Resistivity Index measurement method”, paper SCA 9829 (1998)
2. Jing, X.D., Gillespie, A. and Trewin, B.M.: “Resistivity Index from non-equilibrium measurements using detailed in-situ saturation monitoring”, paper SPE 26798 (1993)
3. www.wipo.int/pctdb/en/wo.jsp?WO=2009138240&IA=EP2009003461&DISPLAY=STATUS
4. Lasswell, P.M., “Core analysis for electrical properties”, Petrophysics, Vol. 47, No. 3, p. 191-213 (2006)
5. www.novocontrol.de
6. Garrouch, A.A. and Sharma M.M., "Techniques for the measurements of electrical properties of cores in the frequency range 10 Hz to 10 MHz”, paper SCA 9211 (1992)
7. McCarthy, J. F., “Effective conductivity of many-component composites by a random walk method”, J. Phys. A: Math. Gen. 23, L749-L753 (1990)
8. Nakashima, Y. and Kamiya, S., “Mathematica programs for the analysis of three-dimensional pore connectivity and anisotropic tortuosity of porous rocks using X-ray computed tomography image data”, J. Nuclear Science and Technology, Vol. 44, No. 9, p. 1233-1247 (2007)

Fig.1 – Left: General view of our 4-contact impedance cell, which consists of two cylindrical shells coaxially sliding one inside the other. Middle: Interior of the cell. Right: Current and voltage electrodes. The voltage electrode is a spring loaded probe that generates a 6N force on the sample face. In order to improve the contact a drop of a soft metal, such as tin or indium, is welded on the tip of the electrode. The diameter of the drop is around 3 mm. The current electrode is a flat corona made of gold-plated brass. Its internal and external diameters are 6 mm and 50.8 mm, respectively. A plastic sheet of gold, not work-hardened by cold processing, is welded on the surface of the corona. Typically, a pressure of 2 bars is applied on it: the contact with the sample face is guaranteed by an independent system of springs that gives the current electrode an additional degree of freedom enabling it to conform to the rock surface very well.

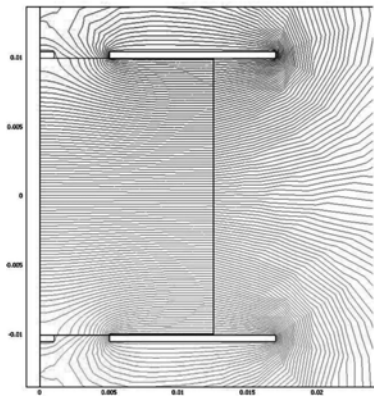

Fig.2 – Equipotential lines in a core sample having a length of 20 mm, a conductivity of 1 mS/m and a dielectric permittivity equal to 40. The electric field frequency is 1 kHz. This numerical simulation was carried out using the Comsol Femlab Multiphysics software. Only half sample is shown for symmetry reasons. The white horizontal rectangles are the electrodes; the black lines are the sample edges. Pictured here is a vertical plane passing through the sample axis. As can be seen, the current electrode is larger than the sample diameter. This minimizes the distortion of the electric field at the lateral edge of the sample. An even potential is consequently generated inside the sample. Notice that the distortion of the field around the voltage electrode has a small extent. It should be noted that although the measured impedance does not depend on the diameter of the sample under test, there is a dependence on the sample length. A calibration curve, obtained by measuring pure brine samples of different thicknesses and known conductivity, is used to correct the measured impedances for this effect.

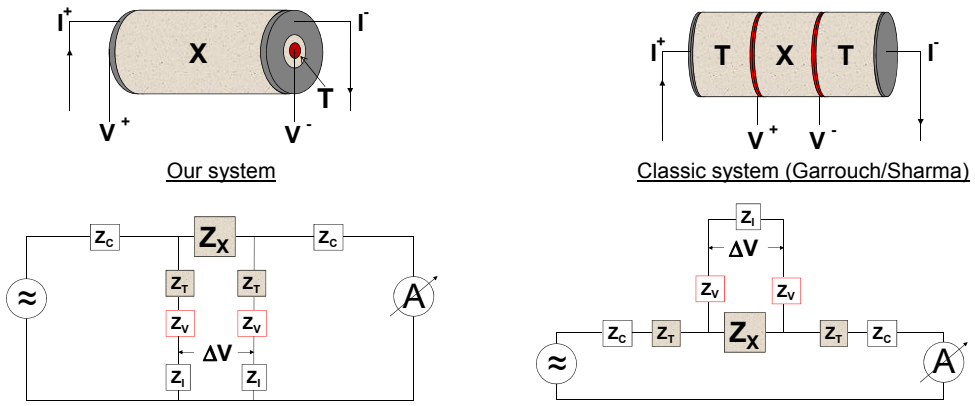

Fig.3 – Equivalent circuits associated with 4-contact measurements. Our system is pictured on the left; the classic system (as described by Garrouch and Sharma [**5**]) is on the right. Both circuits consist of the same impedances, though arranged in different ways. Z_X is the impedance to be measured; Z_I is the internal impedance of the voltmeter; Z_C and Z_V are the impedances associated with the current and voltage electrode/rock interfaces; Z_T is the impedance of that part of rock that lies between the current and the voltage electrode (Z_T is very small in our system). The measurement output is the impedance Z_M, which is defined as the ratio of the measured voltage difference ΔV to the measured current. In both systems Z_M differs from Z_X. The following relations hold:

Our system: $Z_M = Z_X Z_I (Z_C + Z_V + Z_T + Z_I)(Z_V + Z_T + Z_I)^{-2}$

Classic system: $Z_M = Z_X [1 - (2Z_V + Z_X)/(2Z_V + Z_X + Z_I)]$

Z_M differs from Z_X for a non zero current passes through the voltmeter. That happens because voltmeters' internal impedances are not infinite, contrary to what is usually assumed. In our system, errors are caused by the Z_C, Z_V and Z_T impedances. In the classic system they are caused by Z_V and Z_X. The most critical factors are the impedance of the voltage electrode/rock contact (Z_V) and the rock impedance. Although the current electrode/rock contact impedance (Z_C) virtually affects our measurement, it is not a critical factor because it is much smaller than Z_V (the large and flat surface area of the current electrode guarantees a low contact resistance (< 100 Ω) and a high capacitance, thus minimizing Z_C).

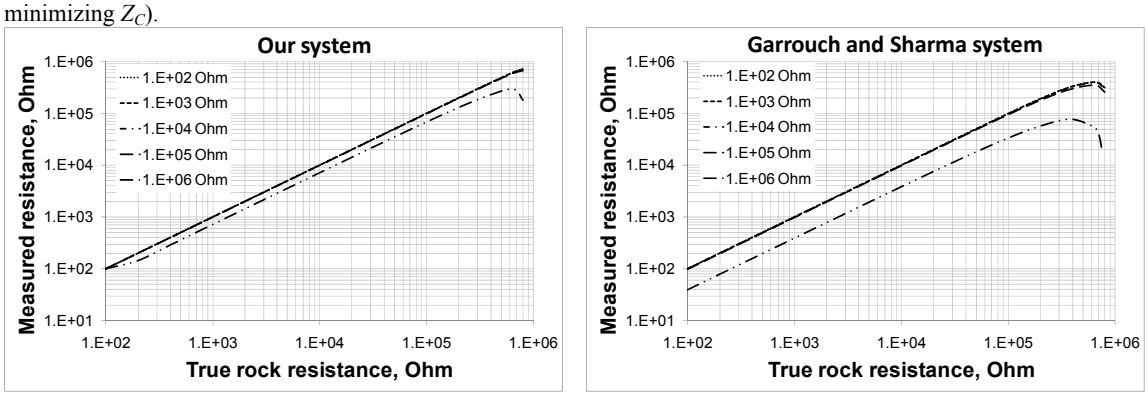

Fig.4 – Measurement errors calculated by solving the circuits shown in **Fig.3**. The plotted curves illustrate the difference between measured and true rock resistance for different values of the resistance of the voltage electrode/rock contact, which is supposed to range from 10^2 Ω to 10^6 Ω and is the most critical factor along with the resistance of the rock. All impedances are treated as combinations of pure resistances and pure capacitances in parallel or in series, and typical values are assigned to them. The following assumptions are made: $Z_X = R$-C in parallel with R ranging from 10^2 Ω to 10^6 Ω and $C = 10^{-10}$ F; $Z_C = R$-C in series with $R = 10^2$ Ω and $C = 10^{-6}$ F; Z_V = pure resistance ranging from 10^2 Ω to 10^6 Ω; $Z_I = R$-C in parallel with $R = 10^{12}$ Ω and $C = 10^{-10}$ F. $Z_T = 10^{-1} \cdot Z_X$ (our system). Our system appears to perform better. The plotted curves were obtained at the standard laboratory frequency of 1 kHz. Higher testing frequencies result in progressively larger errors.

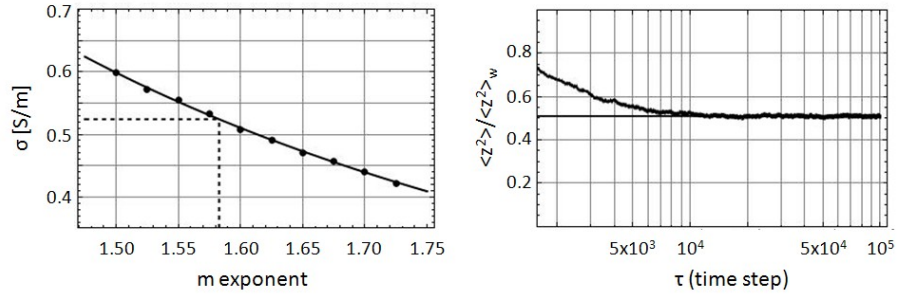

(a) **(b)**

Fig.5 – Outputs of the Random Walk algorithm. (**Fig.5a**): Example of the variation of conductivity as a function of *m* exponent. Dots are the numerically computed conductivities at 10 different *m*-values, while the continuous curve is the best fit to the data with a power law function. The dashed lines represent the extrapolation of the final *m* given the measured conductivity. (**Fig.5b**): Mean-square displacement in the direction of the experimental measurement for a fully-water saturated Berea sandstone, $\langle z^2 \rangle$, normalized by $\langle z^2 \rangle_w$, the mean-square displacement for a lattice walk in free space. The thick solid line describes an average of 10^4 random walkers and the asymptotic value is the final computed value in the long-time limit (10^5 time steps are enough). This asymptotic ratio is proportional to the diffusivity contrast D/D_w and so to the effective conductivity of the sample. The same holds for the *n* exponent and for partially saturated samples.

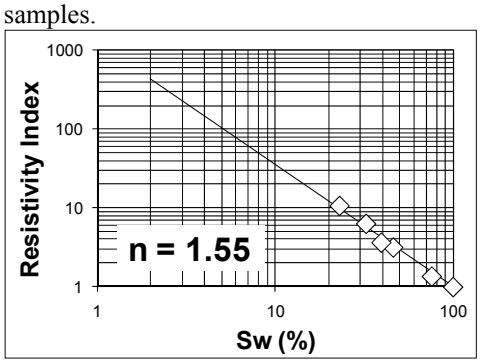

Fig.6 – Resistivity Index curve and Archie n-exponent measured on a Berea sample during a primary-drainage air-brine desaturation in a porous plate cell.

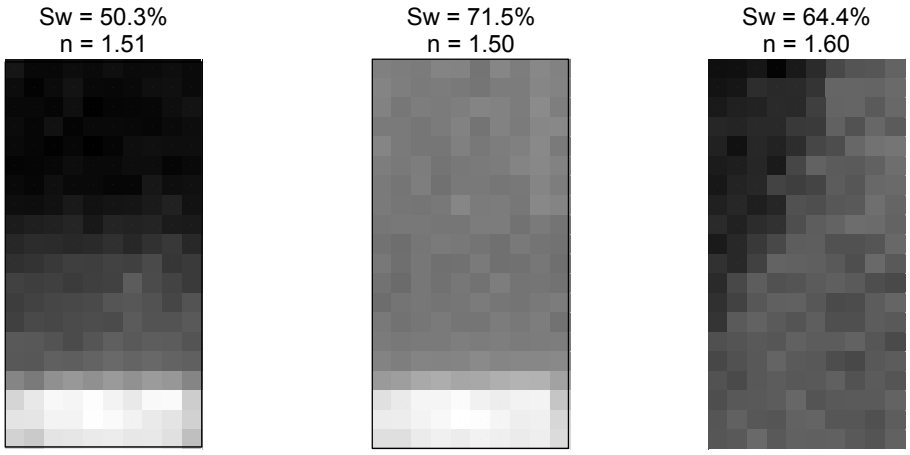

(a) **(b)** **(c)**

Fig.7 – Saturation maps measured on a Berea sample. (**a**) after centrifuging; (**b**) after a long water imbibition; (**c**) after a short water imbibition. The same gray scale is used in the three maps, the black colour corresponding to low water content and the white indicating high water content.

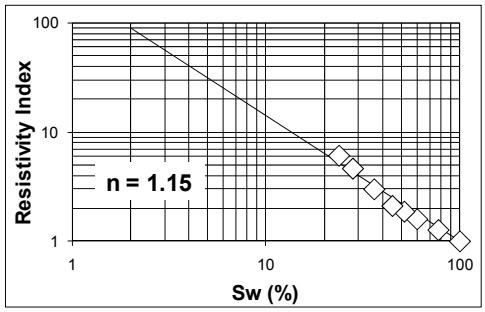

Fig.8 – Resistivity Index curve and Archie n-exponent measured on a laminated sandstone sample using a porous-plate primary-drainage air-brine desaturation.

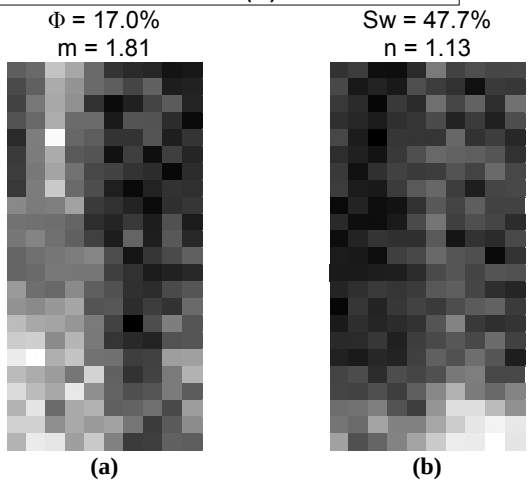

Fig.9 – Porosity (**a**) and Saturation (**b**) maps obtained on a laminated sample before and after centrifuging.

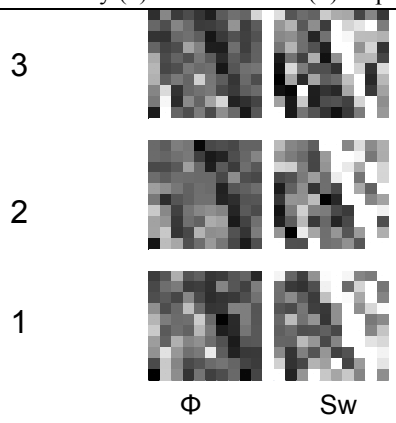

Fig.10 – Three slices showing how porosity (pictured on the left) and Sw (on the right) were distributed in the lower part of the laminated sample of **Fig.9**. As can be seen, colors appear to be distributed in a complementary way: where porosity is high (light gray) Sw is low (dark gray), and vice versa. In the Sw maps on the right, the whitish paths correspond to the fine-grained laminations, which remained fully saturated after sample centrifugation causing quite a low *n* value.

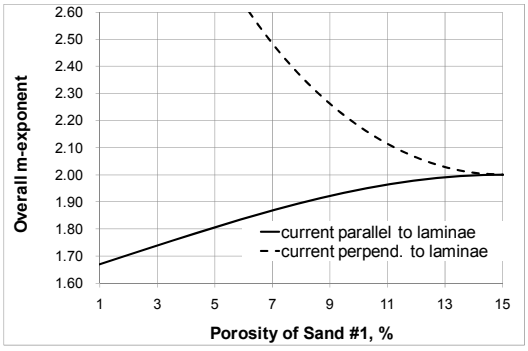

Fig.11 – Theoretical response of a Sand#1/ Sand#2 laminated sample. The overall porosity is 15% and the *m*-exponent equals 2.00 in both sands. Each sand occupies 50% of the bulk volume of the sample. Depending on how porosity is split between the two sands, different overall *m*'s are calculated. This example shows that *m* is scale-dependent. The standard formula $m = -\log(\sigma_w/\sigma_0)/\log(\Phi)$ yields the overall *m* (plug scale); the method we propose in this paper gives also access to the voxel scale (mm).